

Dynamic mass variation and multiphase interaction among steel, slag, lining refractory and nonmetallic inclusions: Laboratory experiments and mathematical prediction

Ju-jin Wang, Li-feng Zhang, Gong Cheng, Qiang Ren, and Ying Ren

Cite this article as:

Ju-jin Wang, Li-feng Zhang, Gong Cheng, Qiang Ren, and Ying Ren, Dynamic mass variation and multiphase interaction among steel, slag, lining refractory and nonmetallic inclusions: Laboratory experiments and mathematical prediction, *Int. J. Miner. Metall. Mater.*, 28(2021), No. 8, pp. 1298-1308. <https://doi.org/10.1007/s12613-021-2304-4>

View the article online at [SpringerLink](#) or [IJMMM Webpage](#).

Articles you may be interested in

Wei-ning Shi, Shu-feng Yang, and Jing-she Li, [Effect of nonmetallic inclusions on localized corrosion of spring steel](#), *Int. J. Miner. Metall. Mater.*, 28(2021), No. 3, pp. 390-397. <https://doi.org/10.1007/s12613-020-2018-z>

Xing Zhao, Hong-liang Zhao, Li-feng Zhang, and Li-qiang Yang, [Gas-liquid mass transfer and flow phenomena in the Peirce-Smith converter: a water model study](#), *Int. J. Miner. Metall. Mater.*, 25(2018), No. 1, pp. 37-44. <https://doi.org/10.1007/s12613-018-1544-4>

Ye-lian Zhou, Zhi-yin Deng, and Miao-yong Zhu, [Study on the separation process of non-metallic inclusions at the steel-slag interface using water modeling](#), *Int. J. Miner. Metall. Mater.*, 24(2017), No. 6, pp. 627-637. <https://doi.org/10.1007/s12613-017-1445-y>

Shi-jian Li, Guo-guang Cheng, Zhi-qi Miao, Lie Chen, and Xin-yan Jiang, [Effect of slag on oxide inclusions in carburized bearing steel during industrial electroslag remelting](#), *Int. J. Miner. Metall. Mater.*, 26(2019), No. 3, pp. 291-300. <https://doi.org/10.1007/s12613-019-1737-5>

Yang Li, Chang-yong Chen, Guo-qing Qin, Zhou-hua Jiang, Meng Sun, and Kui Chen, [Influence of crucible material on inclusions in 95Cr saw-wire steel deoxidized by Si-Mn](#), *Int. J. Miner. Metall. Mater.*, 27(2020), No. 8, pp. 1083-1099. <https://doi.org/10.1007/s12613-019-1957-8>

Sheng-chao Duan, Chuang Li, Han-jie Guo, Jing Guo, Shao-wei Han, and Wen-sheng Yang, [Investigation of the kinetic mechanism of the demanganization reaction between carbon-saturated liquid iron and CaF₂-CaO-SiO₂-based slags](#), *Int. J. Miner. Metall. Mater.*, 25(2018), No. 4, pp. 399-404. <https://doi.org/10.1007/s12613-018-1584-9>



IJMMM WeChat



QQ author group

Dynamic mass variation and multiphase interaction among steel, slag, lining refractory and nonmetallic inclusions: Laboratory experiments and mathematical prediction

Ju-jin Wang¹⁾, Li-feng Zhang²⁾, Gong Cheng¹⁾, Qiang Ren³⁾, and Ying Ren¹⁾

1) School of Metallurgical and Ecological Engineering, University of Science and Technology Beijing, Beijing 100083, China

2) State Key Laboratory of Metastable Materials Science and Technology, Yanshan University, Qinhuangdao 066004, China

3) School of Mechanical Engineering, Yanshan University, Qinhuangdao 066004, China

(Received: 4 March 2021; revised: 10 May 2021; accepted: 12 May 2021)

Abstract: The mass transfer among the multiphase interactions among the steel, slag, lining refractory, and nonmetallic inclusions during the refining process of a bearing steel was studied using laboratory experiments and numerical kinetic prediction. Experiments on the system with and without the slag phase were carried out to evaluate the influence of the refractory and the slag on the mass transfer. A mathematical model coupled the ion and molecule coexistence theory, coupled-reaction model, and the surface renewal theory was established to predict the dynamic mass transfer and composition transformation of the steel, the slag, and nonmetallic inclusions in the steel. During the refining process, Al_2O_3 inclusions transformed into MgO inclusions owing to the mass transfer of $[\text{Mg}]$ at the steel/refractory interface and (MgO) at the slag/refractory interface. Most of the aluminum involved in the transport entered the slag and a small part of the aluminum transferred to lining refractory, forming the Al_2O_3 or $\text{MgO}\cdot\text{Al}_2\text{O}_3$. The slag had a significant acceleration effect on the mass transfer. The mass transfer rate (or the reaction rate) of the system with the slag was approximately 5 times larger than that of the system without the slag. In the first 20 min of the refining, rates of magnesium mass transfer at the steel/inclusion interface, steel/refractory interface, and steel/slag interface were x , $1.1x$, and $2.2x$, respectively. The composition transformation of inclusions and the mass transfer of magnesium and aluminum in the steel were predicted with an acceptable accuracy using the established kinetic model.

Keywords: mass transfer; steel; slag; lining refractory; nonmetallic inclusions; kinetic model

1. Introduction

Mass flow, energy flow, and information flow are the three basic flows of the ironmaking and steelmaking process [1]. For the refining of the steel, complex mass flow occurs during the process as the system is a multiphase and a large number of chemical and physical reactions occur in the system. These mass transfer flow have a significant influence on the composition of inclusions, steel, and slag.

The control of nonmetallic inclusions is an important target during the steel refining process, as inclusions have detrimental effect on the property of steel products [2–3]. Not all inclusions are harmful to the performance of the steel. One of the pivotal factors deciding the influence of inclusions is their composition. Calcium aluminate with large size can cause the fatigue failure in the rolled product of the bearing steel [4]. The MgAl_2O_4 spinel inclusion and some other solid inclu-

sions cause the nozzle clogging during the continue casting process [5]. Some inclusions containing Ti and Mg have positive effect on the toughness of steel [6]. Therefore, it is of a great importance for the accurate control of inclusions.

The slag has an important influence on the composition of the steel and inclusions [7–8]. Shin and Park [9] reported that the mass ratio of $\text{CaO}/\text{Al}_2\text{O}_3$ in refining slag should be controlled between 1.5 and 2.5 to inhibit the formation of solid inclusions in Al deoxidized Mn–V alloyed steel which could ensure the absorption of inclusions by the slag. Ren *et al.* [10–11] proposed the optimized slag of $\text{CaO}\text{--}\text{Al}_2\text{O}_3\text{--}\text{SiO}_2\text{--}\text{MgO}$ slag which was used to modify solid Al_2O_3 inclusions to liquid $\text{CaO}\text{--}\text{Al}_2\text{O}_3\text{--}\text{MgO}$ inclusions. The refractory also has effect on the composition of inclusions in the steel [12], which is often neglected in previous studies [13–15]. Refractory could supply the Mg for the formation of spinel inclusions [16–17]. Reactions between inclusions and re-

fractory have been reported by many researchers [18–21].

To sum up, during the refining process, the molten steel reacts with the slag and refractory continuously, resulting in the constant change of composition of the molten steel. The composition of inclusions also changes accordingly. Shin *et al.* [22] proposed a refractory–slag–metal–inclusions multiphase reaction model and evaluated the influence of slag and refractory on the composition of inclusions. In the model, the mass transfer coefficient of refractory and slag was regressed using the experiment data. Basing on the model proposed by Shin *et al.* [22], Wang *et al.* [23] also established a kinetic model and studied the influence of MgO/ZrO₂/Al₂O₃ refractories on the Ti-containing steel. Although other kinetic models [24–27] have also been established, in these models reactions between the refractory and the molten steel have often been ignored.

In the current study, laboratory experiments were carried out to study the influence of refractory and slag on the mass transfer and composition evolution of the steel and inclusions. Thereafter, a mathematical kinetic model was established to predict the evolution transiently. The mass transfer phenomenon in the model was evaluated using a simplified natural convection heat transfer model.

2. Laboratory experimental setup

Laboratory experiments were carried out using the Fe–1.0C–0.3Si–0.39Mn–1.563Cr–0.0003Mg–0.0015O (wt%) bearing steel and the 51.5CaO–24.3Al₂O₃–7.3SiO₂–6.1MgO–10.8CaF₂ (wt%) pre-melted slag. Two experiments were conducted, one with slag and another without slag. The steel, refractory, and slag reacted with each other for 180 min at 1600°C in a high purity (99.71%) MgO crucible (inner diameter: 42 mm; height: 100 mm) within a Si–Mo furnace under argon atmosphere. The porosity of crucibles was 1.03% according to the test report provided by the Beijing Dingsheng Brothers Technology Co., Ltd., China. After the temperature of the steel reached 1600°C, high purity aluminum (99.999%) was added into the molten steel to control the initial aluminum content to 0.03wt%. After 60 s for the homogenization of the steel, a water-cooled sample was taken out and 25 g pre-melted slag was added on the surface of the steel. Then, steel samples and slag samples were taken at specific intervals.

Steel samples were prepared for the composition and inclusions analysis. The content of total oxygen (T.O) was detected using a LECO ONH analyzer, and the dissolved aluminum ([Al]) and total magnesium (T.Mg) were determined using inductively coupled plasma atomic emission spectrometry (ICP-AES). The composition of slag was analyzed using X-ray fluorescence spectrometry (XRF). Inclusions analysis was using an automatic scanning electron microscope equipped with an energy dispersive spectrometer (SEM–

EDS) with an acceleration voltage of 20 kV and a spot size of 35%. The detection limit of inclusion diameter was 1 μm.

3. Model mathematical formulation

3.1. Thermodynamic and kinetic models

The current model was based on the coupled-reaction model [25,27–28], and reactions between the steel and the refractory were taken into account. Reactions listed in Table 1 were considered at the steel/slag and steel/inclusion interfaces to predict the evolution of inclusions. At the steel/refractory interface, the equilibrium between the dissolved [Mg] and [O] in the steel and the solid magnesium oxide in the refractory ((MgO)_s) was also considered. It was assumed that the refractory only dissolved into the slag, and no chemical reaction occurred at the refractory/slag interface.

Table 1. Reactions considered at the interfaces of steel/slag and steel/inclusion [29]

Reaction	$\Delta G^\ominus / (\text{J} \cdot \text{mol}^{-1})$
[Ca] + [O] = (CaO)	$\Delta G_{\text{Ca}}^\ominus = -645200 + 148.7T$
2[Al] + 3[O] = (Al ₂ O ₃)	$\Delta G_{\text{Al}}^\ominus = -1206220 + 390.39T$
[Si] + 2[O] = (SiO ₂)	$\Delta G_{\text{Si}}^\ominus = -581900 + 221.8T$
[Mn] + [O] = (MnO)	$\Delta G_{\text{Mn}}^\ominus = -244300 + 107.6T$
[Mg] + [O] = (MgO)	$\Delta G_{\text{Mg}}^\ominus = -89960 - 82.0T$

Note: ΔG^\ominus —standard Gibbs free energy; T —temperature.

The thermodynamic equilibrium was assumed at the interface, and the equilibrium was solved using the coupled-reaction model. A general expression for reactions at the steel/slag interface and steel/inclusion interface was as follows.

$$[M] + n[O] = (\text{MO}_n) \quad (1)$$

where M represents elements in the steel, Ca, Al, Si, Mn, Mg, etc.; n represents the stoichiometric number of O in MO_{*n*}.

When the reaction is at the equilibrium state, then:

$$\Delta G = \Delta G^\ominus + RT \ln \frac{a_{\text{MO}_n}}{a_{[M]} a_{[O]}^n} = 0 \quad (2)$$

where ΔG is the change of free Gibbs energy, J·mol⁻¹; R is the ideal gas constant, which is equal to 8.314 J·mol⁻¹·K⁻¹; T is the temperature, K; a is the activity of components.

The activity of components in the molten steel was calculated according to the Wagner Interaction Parameter Formalism (WIPF) [30–31], as shown in Eq. (3). A few second-order interaction parameters were employed in the calculation for more accurate calculated results, even though only a small number of parameters were available in the literature.

$$\lg f_M = \sum_{j=2}^n e_M^j [\%j] + \sum_{j=2}^n \sum_{l=2}^n r_M^{jl} [\%j][\%l] \quad (3)$$

where f_M is the activity coefficient of M; e and r are the first-order and second-order interaction parameters, respectively,

as listed in Table 2; j and l are components of the molten steel Fe–C–Si–Mn–Cr–O–Ca–Al–Mg, so $n = 9$; $[\%j]$ and $[\%l]$ are the content of j and l in the steel, wt%. The standard state was chosen as 1wt%.

The activity of MO_n in the slag or inclusions was calculated according to the Ion and Molecular Coexistence Theory (IMCT) [35–37]. The activity of solid oxide at the steel/refractory interface was set to be 1.0. Although the slag used in the current study was CaO–Al₂O₃–SiO₂–MgO–CaF₂ system, which did not contain MnO, a slag consisted of CaO–Al₂O₃–SiO₂–MnO–MgO–CaF₂ was employed to calculate the activity. This is because the steel contained 0.39wt% Mn, and MnO might be formed during the reaction process. There are six simple structural units and 26 complex molecules in this slag system according to the IMCT, as listed in Table 3. The detailed calculation measure can be found in the authors' previous work [34].

As reactions at the interface are at the equilibrium state, a

concentration gradient occurs between the bulk and interface. This concentration gradient is the driving force of the components' diffusion, which could be calculated according to Eqs. (4)–(5):

$$J_M = \frac{1000k_M \cdot \rho_{\text{steel}}}{100M_M} \left([\%M]^b - [\%M]^* \right) \quad (4)$$

$$J_{MO_n} = \frac{1000k_{MO_n} \cdot \rho_{\text{slag(or inclusion)}}}{100M_{MO_n}} \left((\%MO_n)^* - (\%MO_n)^b \right) \quad (5)$$

where J is the molar flux density, mol·m⁻²·s⁻²; k_M and k_{MO_n} are the mass transfer coefficients of the M and MO_n , respectively, m·s⁻¹; ρ_{steel} is the steel density, kg·m⁻³; ρ_{slag} is the slag density, kg·m⁻³; $\rho_{\text{inclusion}}$ is the inclusion density, kg·m⁻³; M is the molecular weight, g·mol⁻¹; $(\%MO_n)$ is the content of MO_n in the slag or inclusion, wt%; the superscript b and $*$ represent the bulk and interface, respectively.

Under the assumption that no material accumulates at the

Table 2. Some activity interaction coefficients of elements in the molten steel [32–34]

M	e_M^j							
	Al	C	Ca	Cr	Mg	Mn	O	Si
Al	63/T + 0.011	0.091	-0.047	0.012	-0.13	0	-34740/T + 11.95	0.056
C	0.043	158/T + 0.0581	-0.097	-0.023	-0.07	-0.012	-0.34	162/T - 0.008
Ca	-0.072	-0.34	-0.002	0.02	0	-0.0156	-2500	-0.097
Cr	0.023	-0.12	0.026	-0.0003	0.1	0.0039	-0.14	-0.0043
Mg	-0.12	-0.15	0	-0.0003	0	0	-289	-0.09
Mn	0	-0.07	-0.023	0.05	0	0	-0.083	-0.00026
O	-20600/T + 7.15	-0.45	-990	-0.04	-190	-0.021	-1750/T + 0.734	-0.131
Si	0.058	380/T - 0.023	-0.067	-0.0003	-0.105	0.002	-0.23	34.5/T + 0.089
M	r_M^{jj}							
	Al	C	Ca	Cr	Mg	Mn	O	Si
Al	0.17/T - 0.0011	-0.004	—	—	—	—	—	-0.0006
C	-0.0007	8.94/T + 0.0026	—	—	—	—	—	11.94/T - 0.0003
Ca	0.0007	0.012	—	—	—	—	2.6 × 10 ⁵ , 2.1 × 10 ⁵ *	0.0009
Cr	—	—	—	—	—	—	—	—
Mg	—	—	—	—	—	—	—	—
Mn	—	—	—	—	—	—	—	—
O	1.7	—	4.2 × 10 ⁴ , 2.1 × 10 ⁵ *	0.00037	—	—	—	—
Si	—	—	—	—	—	—	—	6.5/T - 0.0055

Note: the superscript * represents the value was r_M^{Mj} .

Table 3. Structural units in the CaO–MgO–CaF₂–Al₂O₃–SiO₂–MnO slag according to the IMCT [34]

Simple compounds	Complex compounds
(Ca ²⁺ + O ²⁻); (Mg ²⁺ + O ²⁻); (Ca ⁺ + 2F ⁻); Al ₂ O ₃ ; SiO ₂ ; MnO.	3CaO·SiO ₂ ; 2CaO·SiO ₂ ; 3CaO·2SiO ₂ ; CaO·SiO ₂ ; 3CaO·Al ₂ O ₃ ; 12CaO·7Al ₂ O ₃ ; CaO·Al ₂ O ₃ ; CaO·2Al ₂ O ₃ ; CaO·6Al ₂ O ₃ ; 2MgO·SiO ₂ ; MgO·SiO ₂ ; MgO·Al ₂ O ₃ ; 2MnO·SiO ₂ ; MnO·SiO ₂ ; MnO·Al ₂ O ₃ ; 3Al ₂ O ₃ ·2SiO ₂ ; 3CaO·MgO·2SiO ₂ ; 2CaO·MgO·2SiO ₂ ; CaO·MgO·SiO ₂ ; CaO·MgO·2SiO ₂ ; 2CaO·Al ₂ O ₃ ·SiO ₂ ; CaO·Al ₂ O ₃ ·2SiO ₂ ; 3CaO·2Al ₂ O ₃ ·CaF ₂ ; 11CaO·7Al ₂ O ₃ ·CaF ₂ ; 3CaO·2SiO ₂ ·CaF ₂ ; 2MgO·2Al ₂ O ₃ ·5SiO ₂ .

interface, the molar flux densities of the slag and steel are equal to each other, as shown in Eq. (6).

$$J_M = J_{MO_n} \quad (6)$$

Moreover, Eq. (7) is the electric neutral equation, showing the flux density of cations is equal to that of anions.

$$J_{Ca} + 1.5J_{Al} + 2J_{Si} + J_{Mn} + J_{Mg} - J_O = 0 \quad (7)$$

Coupling Eqs. (2)–(7), the concentration of components at the interface could be solved, and then the mass transfer between the bulk and the steel/slag interface in time dt was calculated as Eqs. (8)–(9) [25,27,38].

$$\frac{d[\%M]}{dt} = -\frac{A_{\text{interface}} \cdot k_M}{V_{\text{steel}}} \left([\%M]^b - [\%M]^* \right) \quad (8)$$

$$\frac{d(\%MO_n)}{dt} = -\frac{A_{\text{interface}} \cdot k_{MO_n}}{V_{\text{slag}}} \left[(\%MO_n)^b - (\%MO_n)^* \right] \quad (9)$$

where, t is the time, s; $A_{\text{interface}}$ is the area of interface, m^2 ; V is the volume, m^3 .

Reactions occurred at the steel/inclusions interface were similar to those at the steel/slag interface. The difference lied in the characteristics of the interface. The mass transfer between the bulk and the steel/inclusions interface was calculated as Eqs. (10)–(11).

$$\frac{d[\%M]}{dt} = -\frac{P_{3D} \cdot A_{\text{interface}} \cdot k_M}{V_{\text{steel}}} \left([\%M]^b - [\%M]^* \right) \quad (10)$$

$$\frac{d(\%MO_n)}{dt} = -\frac{6 \cdot k_{\text{inclusion}}}{d_{\text{inclusion}}} \left[(\%MO_n)^b - (\%MO_n)^* \right] \quad (11)$$

where, P_{3D} is number density of inclusions in three dimension, m^{-3} ; $d_{\text{inclusion}}$ is the diameter of inclusion, m.

As for reactions at the steel/refractory interface, only the generation and decomposition of MgO and Al_2O_3 were considered. The MgO crucible used in the current study was quite dense, so that the absorption of inclusions by the crucible was ignored. What's more, the spalling of the crucible maybe occurred at the steel/refractory interface [39–40], which was not considered due to the high purity of the crucible. Only the spalling or dissolution of refractory at the slag/refractory interface was taken into account, and an overall variation of slag composition caused by the slag/refractory reaction was estimated, no matter with the dissolution or the spalling.

3.2. Determination of mass transfer coefficients

Owing to the shape difference among the steel/inclusion interface, the steel/slag interface, the steel/refractory interface, and the slag/refractory interface, the mass transfer at these phases are different, implying different models to calculate the mass transfer coefficient (MTC) within these phases.

The surface renewal theory [41] was employed to calculate the MTC at steel/inclusion interface. According to the surface renewal theory, there are numerous fluid eddies with different residence time at the interface. The substance at the interface was constantly replaced and updated in the process

of fluid flow. The MTC at steel/inclusion interface was calculated from Eq. (12), suggested by Harada *et al.* [27].

$$k_{M_inc} = \frac{1}{10} \sqrt{\frac{2D_M u_{\text{slip}}}{\pi d_{\text{inclusion}}}} \quad (12)$$

where, k_{M_inc} is the mass transfer coefficient of M at the steel/inclusion interface, $m \cdot s^{-1}$; D_M is the diffusivity coefficient, $m^2 \cdot s^{-1}$, as listed in Table 4; u_{slip} is the slip velocity between the inclusion and the molten steel, which was calculated using Eq. (13) [27], $m \cdot s^{-1}$.

Table 4. Diffusivity coefficients of components in the molten steel and slag

Component	$D / (10^{-9} m^2 \cdot s^{-1})$
Mg, Al, Si	22.36
Mn, Ca	18.83
MgO, CaO, MnO	2.03
SiO_2, Al_2O_3	2.08

Note: values were from published references [42–44]

$$u_{\text{slip}} = \frac{(\rho_{\text{steel}} - \rho_{\text{inclusion}}) d_{\text{inclusion}}^2 g}{18 \mu_{\text{steel}}} \quad (13)$$

where, g is acceleration of gravity, $g = 9.8 m \cdot s^{-2}$; μ_{steel} is the viscosity of steel, $kg \cdot m^{-1} \cdot s^{-1}$.

For the other three types interfaces, the MTC was calculated as Eq. (14) [45–46] shows.

$$k_M = c D_M^{0.5} \left(\frac{\varepsilon}{\nu} \right)^{0.25} \quad (14)$$

where, c is a constant, $c = 0.4$ at the refractory/slag and refractory/steel interface, and $c = 2.0$ at the steel/slag interface; ε is the turbulent dissipation rate, $m^2 \cdot s^{-3}$; ν is the kinematic viscosity, $m^2 \cdot s^{-1}$.

To obtain the value of ε , a simplified natural heat transfer model was established. The geometry of the computational domain is shown in Fig. 1. In the model, the effect of temperature on the density of molten steel was described using the Boussinesq model, as shown in Eq. (15). The heat transfer rate at the top surface was $-15 kW \cdot m^{-2}$, and that at the bottom surface was $-1.4 kW \cdot m^{-2}$. The temperature at the side wall was set to be a constant, which was equal to 1873 K. Other parameters used in the simulation are listed in Table 5. The commercial CFD software, Fluent 17.0, was used to simulate the distribution of temperature and turbulent properties under steady state. Calculated results are shown in Fig. 2. The temperature of the steel was range from 1860 to 1873 K. There was a coolest region at the center of top surface, which was below 1870 K. The temperature increased gradually with this coolest as the center. A similar condition was at the bottom surface. Fig. 2(b) shows the contour of turbulent dissipation rate. The average stirring energy of the steel at the top surface was $8.28 \times 10^{-8} m^2 \cdot s^{-3}$, and that at the bottom and the side were $1.06 \times 10^{-8} m^2 \cdot s^{-3}$ and $3.35 \times 10^{-8} m^2 \cdot s^{-3}$, respectively.

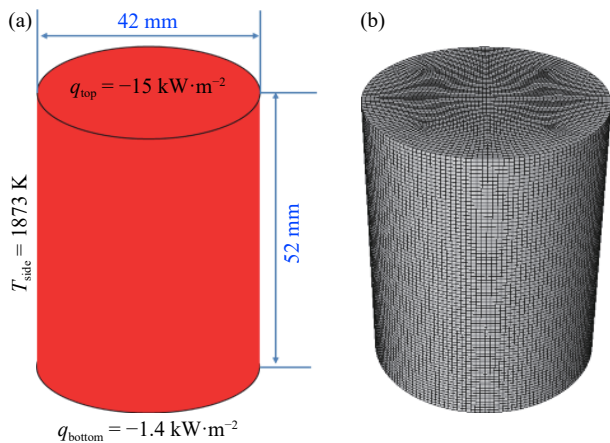


Fig. 1. Geometry and mesh of the computational domain: (a) geometry; (b) mesh.

$$(\rho - \rho_0)g = -\rho_0\beta(T - T_0)g \quad (15)$$

where, ρ and ρ_0 are the density of the molten steel at temperature of T and T_0 , $\text{kg}\cdot\text{m}^{-3}$; β is the thermal expansion coefficient of the molten steel, K^{-1} .

3.3. Other parameters

Using the models established above, the mass transfer of elements during the refining process was analyzed. Other parameters used in the model are summarized in Table 6, where the saturated solubility of MgO in the slag was as-

sumed to be 17wt%. Two laboratory situations were calculated to analyze the mass transfer flow. One was the refining system without slag, and the other was the system with slag.

4. Dynamic mass transfer in the system of steel–lining refractory–nonmetallic inclusions

Fig. 3 shows the evaluation of inclusions composition over time in the system without slag. Primary inclusions in the steel had a high content of Al_2O_3 , and there was also a small amount of $\text{CaO}\text{--}\text{Al}_2\text{O}_3\text{--}\text{MgO}$ inclusions with melting point lower than 1873 K. When reacting for 60 min, pure Al_2O_3 inclusions disappeared in the steel, and some $\text{MgO}\cdot\text{Al}_2\text{O}_3$ inclusions with small diameter generated. Increasing the reacting time to 120 min, the content of Al_2O_3 in inclusions was further reduced, and at the same time, a more amount of spinel was formed in the steel. The size of inclusions in the sample of “180 min” had a sharp decrease. The maximum diameter of inclusions in the steel after holding for 180 min was as small as 3.2 μm , implying an efficient removal of large inclusions within 180 min.

As the raw material used in the study was taken from the bloom, where inclusions could be assumed to be in thermodynamic equilibrium with the steel, the increase of content of MgO in inclusions was because of the increase of [Mg] in the steel. And there was no slag in the system, so reactions between the molten steel and the refractory supplied the

Table 5. Parameters employed in the simulation

Property	Value
Density of the molten steel, $\rho_{\text{steel}} / (\text{kg}\cdot\text{m}^{-3})$	7000
Viscosity of the molten steel, $\mu_{\text{steel}} / (\text{Pa}\cdot\text{s})$	0.0067
Heat capacity of the molten steel, $C_{p,\text{steel}} / (\text{J}\cdot\text{kg}^{-1}\cdot\text{K}^{-1})$	823.6
Thermal conductivity of the molten steel, $\lambda_{\text{steel}} / (\text{J}\cdot\text{m}^{-1}\cdot\text{s}^{-1}\cdot\text{K}^{-1})$	40.3
Thermal expansion coefficient of the molten steel, $\beta_{\text{steel}} / \text{K}^{-1}$	4.4×10^{-6}

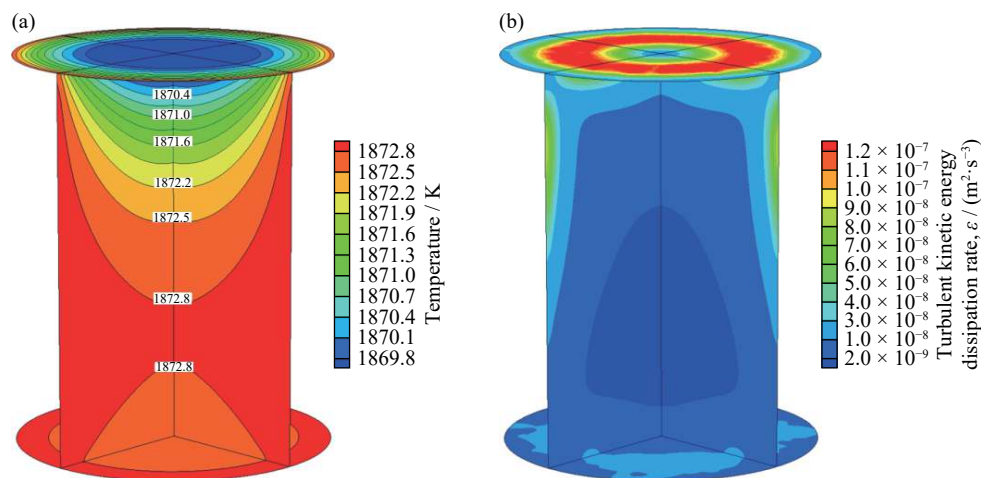


Fig. 2. Calculated temperature and kinetic turbulent energy of the molten steel in the heated crucible: (a) temperature contour; (b) turbulent kinetic energy dissipation rate contour.

Table 6. Additional parameters used in the model

Property	Value
Density of the slag, $\rho_{\text{slag}} / (\text{kg} \cdot \text{m}^{-3})$	3000
Density of the inclusion, $\rho_{\text{inclusion}} / (\text{kg} \cdot \text{m}^{-3})$	3500
Density of the MgO refractory, $\rho_{\text{ref}} / (\text{kg} \cdot \text{m}^{-3})$	3400 [23]
Saturated solubility of MgO in the slag, $(\text{MgO})_{\text{sat}} / \text{wt}\%$	17
Kinematic viscosity of the slag, $\nu_{\text{slag}} / (\text{m}^2 \cdot \text{s}^{-1})$	3.5×10^{-5}
Diameter of the inclusion, $d_{\text{inclusion}} / \text{m}$	2.0×10^{-6}
Two-dimensional number density of inclusions, P_{2D} / m^{-2}	1.09×10^7

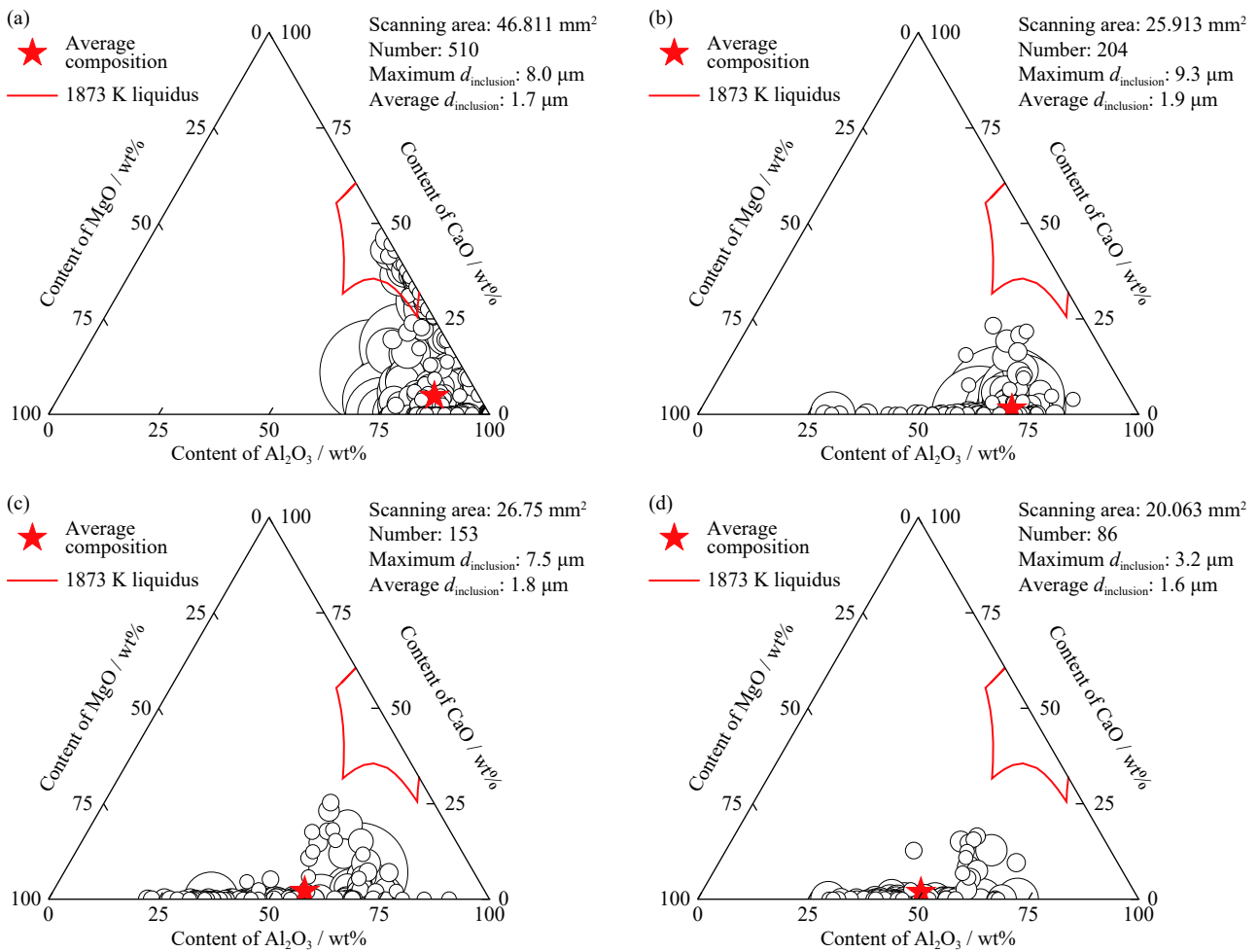


Fig. 3. Evolution of inclusions composition in the system of steel–inclusion–refractory after different reaction times: (a) 0 min; (b) 60 min; (c) 120 min; (d) 180 min.

[Mg], which was often neglected in the literature [13–14]. In order to study quantitatively the transfer process of [Mg] from the refractory to the molten steel, the calculated kinetic results are shown in Fig. 4. Fig. 4(a) is the evolution of steel composition, and Fig. 4(b) is that of inclusions composition. With the increase of holding time, the content of Al_2O_3 in inclusions decreased gradually, while the content of MgO had an opposite rise trend. The experimental results were accurately reproduced by the current kinetic model. As to the com-

position of the molten steel, the content of total Al (T.Al) had a decrease, which was thought to be replaced by the MgO in the refractory, as Eq. (16) shows. Fig. 5 shows the element distribution at the interface between the molten steel and the MgO refractory when holding for 180 min. $\text{MgO} \cdot \text{Al}_2\text{O}_3$ inclusions and inclusions with high content of Al_2O_3 were observed at the interface, which also verified the occurrence of Eq. (16) at the interface. The absorption of inclusions by the refractory at the interface was not considered as the content

of Mg in inclusions was quite higher than that at the interface where the content of Al was high.

$$[\text{Al}] + (\text{MgO}) = [\text{Mg}] + (\text{Al}_2\text{O}_3) \quad (16)$$

5. Dynamic mass transfer in the system of steel–slag–lining refractory–nonmetallic inclusions

To study the influence of the slag on the mass flow during the refining process, a laboratory experiment and numerical simulation on the system with the slag was also conducted. The experimental evolution of inclusions composition over time is shown in Fig. 6. With the increase of holding time, inclusions in the molten steel transformed from Al_2O_3 into $\text{MgO} \cdot \text{Al}_2\text{O}_3$ and then pure MgO. Most of inclusions changed

into pure MgO after holding for 60 min.

Comparisons of the composition evolution of the slag, inclusions and the steel between experimental results and predicted ones are shown in Fig. 7. The change of the slag composition was mainly owing to the dissolution of MgO from the refractory. The composition of inclusions changed quite faster in the system with slag than that without slag. It took about 30 min for reactions in the system with slag to reach the equilibrium, while reactions in the slag free system hardly reached the equilibrium even after 180 min. The slag had an apparent acceleration effect on the mass transfer during the refining, as shown in Fig. 8. The transformation rate of inclusions in the system with slag was about 5 times faster than that without slag. The slag absorbed MgO from the refractory, and then transferred Mg to the molten steel at the

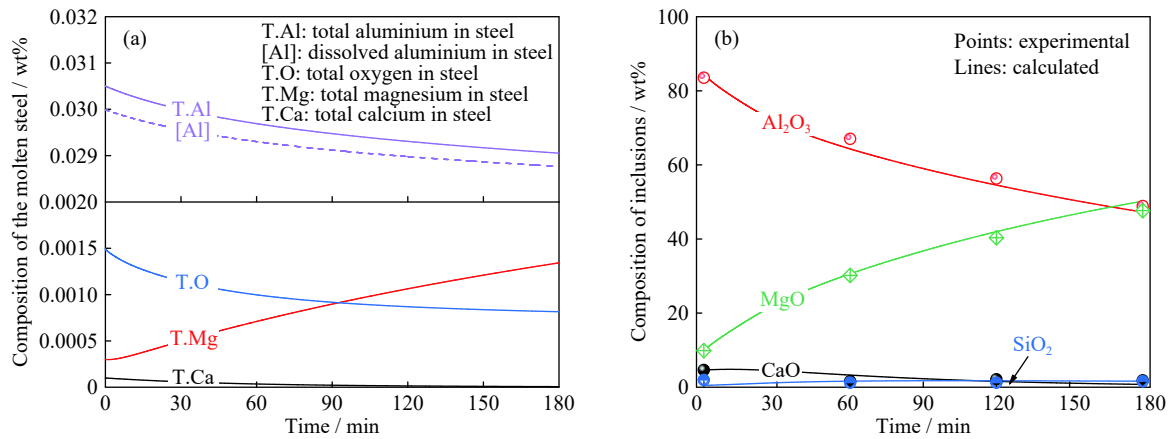


Fig. 4. Evolution of composition of (a) steel and (b) inclusions.

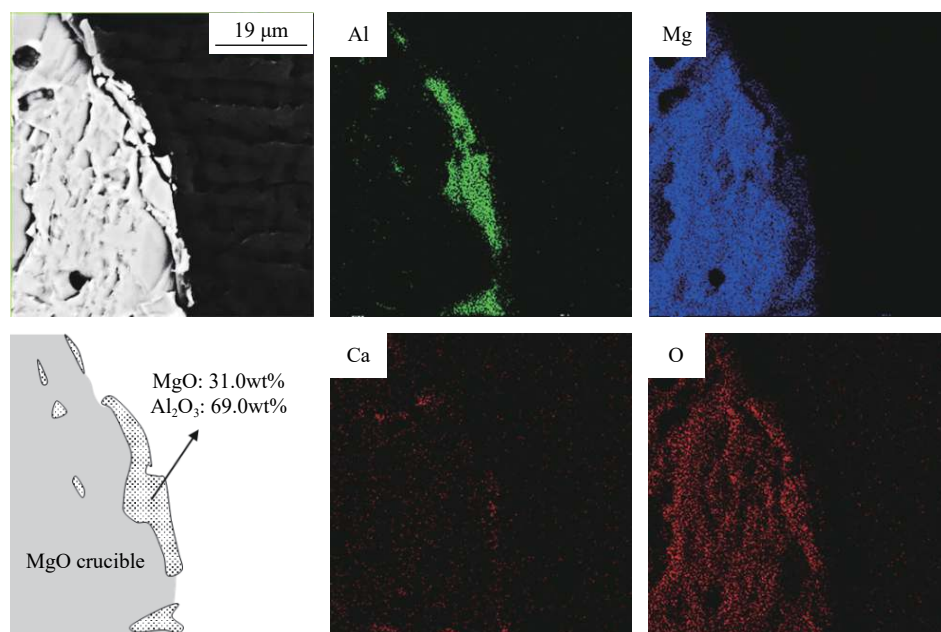


Fig. 5. Elements distribution at the steel/refractory interface when holding for 180 min.

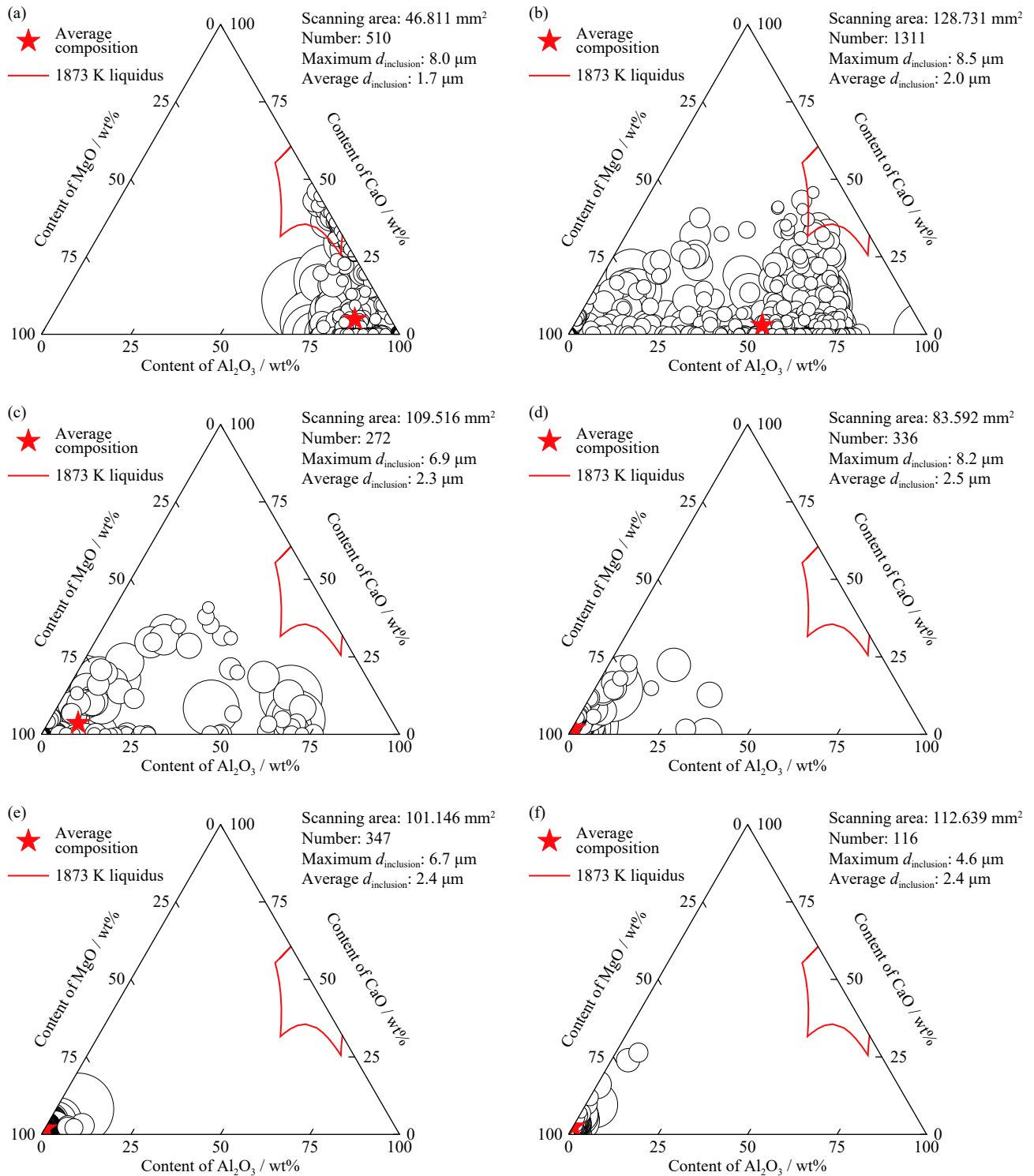


Fig. 6. Evolution of inclusions composition in the system of steel–slag–inclusion–refractory after different reaction times: (a) 0 min; (b) 15 min; (c) 30 min; (d) 60 min; (e) 120 min; (f) 180 min.

steel/slag interface. Besides, the slag could also affect the final equilibrium state of reactions in the system. In the current refining system, the aluminum kept transferring from the steel to the refractory and slag, while the magnesium kept transferring from the refractory to the steel with the form of

[Mg] and to the slag with the form of (MgO). The MgO in the slag then reacted with the steel, transferring Mg to the molten steel. The content of T.Mg in the steel had a slow decrease after holding for 60 min, as shown in Fig. 7(c), which was not predicted by the kinetic model. This is because the floatation

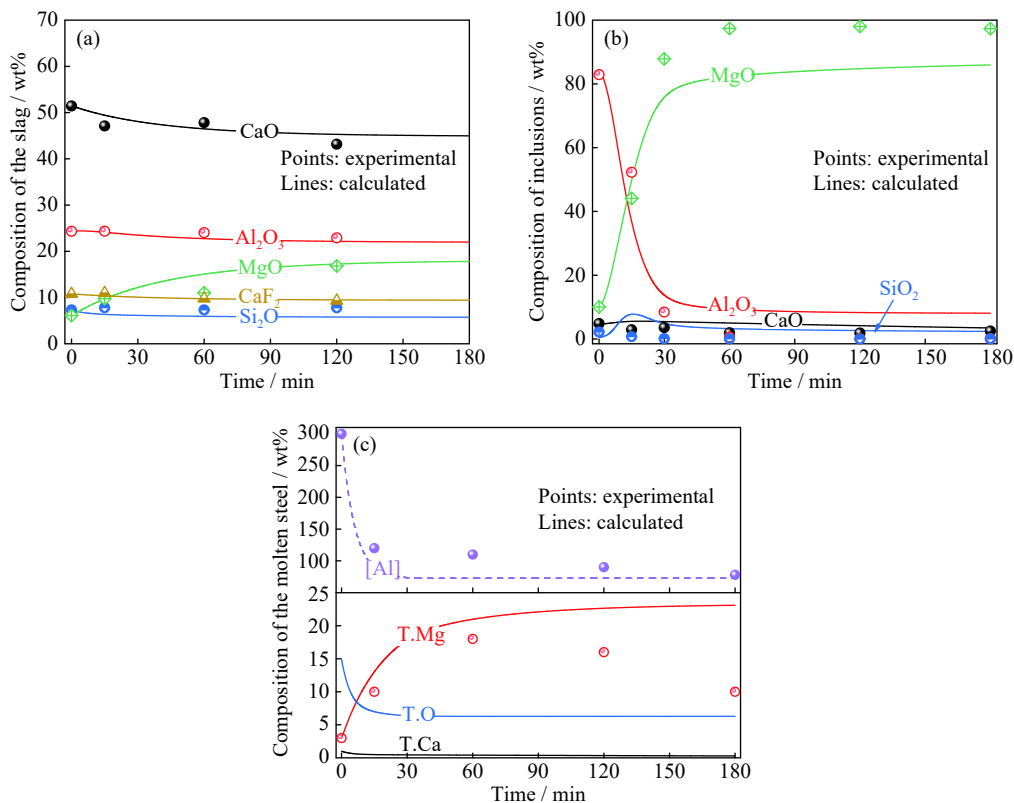


Fig. 7. Comparisons between experimental results and the predicted ones: (a) slag composition; (b) inclusions composition; (c) steel composition.

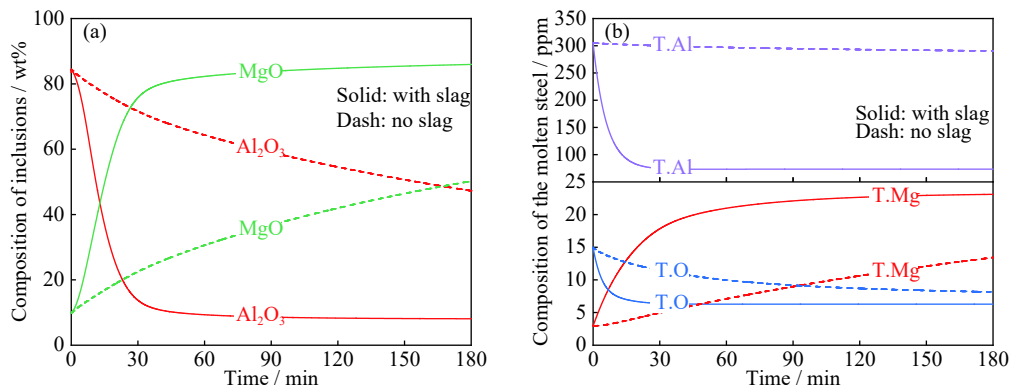


Fig. 8. Acceleration of the slag on the mass transfer: (a) composition of inclusions; (b) composition of the steel.

removal of inclusions was not considered in the current model. With floatation removal of inclusions, it is apparent that the T.Mg and T.Al in the steel declined with the holding time.

It was concluded that there were two ways for the entrance of Mg into the molten steel. The mass transfer process of Mg ([Mg] or MgO) is shown in Fig. 9. The dissolution rate of MgO from the refractory to the slag was the fastest, which was larger than 3×10^{-3} wt%/s within the first 20 min. The mass transfer rate of [Mg] from the slag to the steel in the first 20 min was approximately 7.04×10^{-7} wt%/s in average. And that from the refractory to the steel and from inclusions to the steel were about 3.54×10^{-7} wt%/s and -3.16×10^{-7} wt%/s,

respectively.

The overall mass transfer of Mg and Al are shown in Fig. 10. The mass transfers of Mg and Al through direct steel–refractory reactions were a little slow. The slag phase in the system played a role like a catalyzer, accelerating both the dissolution of MgO at the slag/refractory interface and steel–slag reactions, resulting the faster mass transfer rate of Mg from the refractory. In the first 20 min of the refining, if the mass transfer rate of magnesium from the steel to inclusions was taken as x , then the rates of magnesium mass transfer at the steel/refractory interface and at the steel/slag interface were $1.1x$, and $2.2x$, respectively.

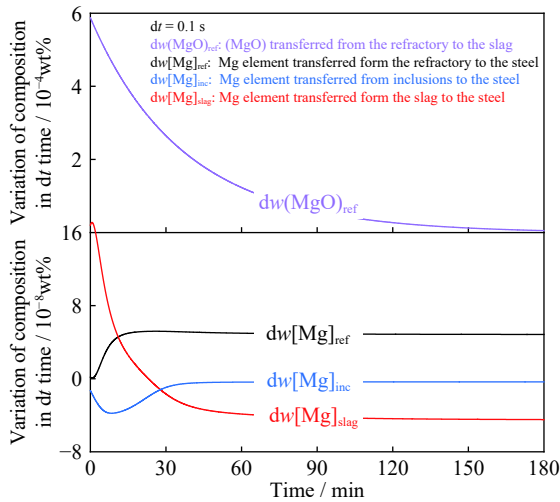


Fig. 9. Mass transfer process of Mg ([Mg] or MgO).

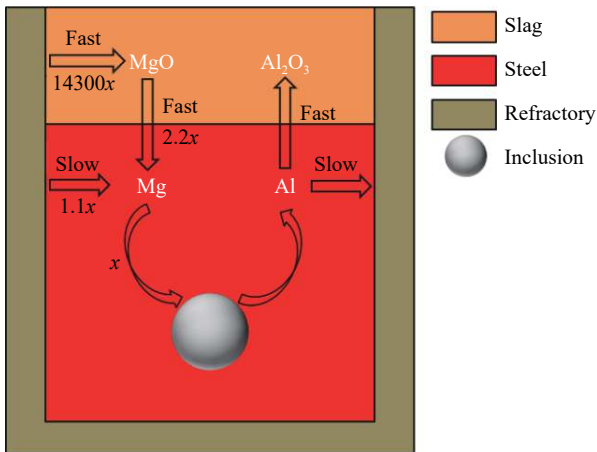


Fig. 10. Overall mass transfer of Mg and Al during the refining.

6. Conclusions

In the current study, the mass transfer flow in the refining process of a bearing steel was analyzed using laboratory experiments and numerical kinetic prediction. The following conclusions were derived.

(1) During the refining process, magnesium transferred from the refractory into the molten steel through two ways. One was reactions between the refractory and the steel, and another was steel–slag reactions, where the MgO was mainly originated the dissolution of refractory. Most of the aluminum involved in the transport entered the slag and a small part of the aluminum transferred to refractory, forming the Al_2O_3 or $MgO \cdot Al_2O_3$.

(2) The slag had an apparent acceleration on the mass transfer. The mass transfer rate in the system with the current slag was about 5 times faster than that without slag. It took about 30 min for reactions in the system with slag to reach the equilibrium, while reactions in the slag free system hardly reached the equilibrium even after 180 min.

(3) A kinetic model for predicting the mass transfer and composition transformation of the refractory–steel–slag–inclusion multiphase was established based on the coupled reaction model. The experimental results were well reproduced using the model.

(4) The mass transfer rate of magnesium varied with the interface. In the first 20 min of the refining, the rates of magnesium mass transfer at the steel/inclusion interface, steel/refractory interface, and the steel/slag interface were x , $1.1x$ and $2.2x$, respectively.

Acknowledgements

This work was financially supported by the National Natural Science Foundation China (Nos. U1860206, 51725402, and 51874032), the Fundamental Research Funds for the Central Universities (Nos. FRF-TP-19-037A2Z and FRF-BD-20-04A), the S&T Program of Hebei, China (No. 20311006D), the High Steel Center (HSC) at Yanshan University, China, and the High Quality Steel Consortium (HQSC) at University of Science and Technology Beijing, China.

References

- [1] R.Y. Yin, *Metallurgical Process Engineering*, Springer, Berlin, Heidelberg, 2011, p. 26.
- [2] L.F. Zhang, *Non-Metallic Inclusions in Steels: Fundamentals*, Metallurgical Industry Press, 2019, p. 320.
- [3] L.F. Zhang, *Non-metallic Inclusions in Steels: Industrial Practice*, Metallurgical Industry Press, Beijing, 2019, p. 482.
- [4] C. Gu, J.H. Lian, Y.P. Bao, Q.G. Xie, and S. Munstermann, Microstructure-based fatigue modelling with residual stresses: Prediction of the fatigue life for various inclusion sizes, *Int. J. Fatigue*, 129(2019), art. No. 105158.
- [5] Y.P. Chu, Z.Y. Chen, N. Liu, and L.F. Zhang, Formation and control of spinel inclusions in high-speed heavy rail steel, *Iron Steel*, 55(2020), No. 1, p. 38.
- [6] M.M. Song, C.L. Hu, B. Song, H.Y. Zhu, Z.L. Xue, and R.S. Xu, Effect of Ti–Mg treatment on the impact toughness of heat affected zone in 0.15%C–1.31%Mn steel, *Steel Res. Int.*, 89(2018), No. 3, art. No. 1700355.
- [7] J.F. Xu, K.P. Wang, Y. Wang, Z.D. Qu, and X.K. Tu, Effects of ferrosilicon alloy, Si content of steel, and slag basicity on compositions of inclusions during ladle furnace refining of Al-killed steel, *J. Iron Steel Res. Int.*, 27(2020), No. 9, p. 1011.
- [8] S.J. Li, G.G. Cheng, Z.Q. Miao, L. Chen, and X.Y. Jiang, Effect of slag on oxide inclusions in carburized bearing steel during industrial electroslag remelting, *Int. J. Miner. Metall. Mater.*, 26(2019), No. 3, p. 291.
- [9] J.H. Shin and J.H. Park, Effect of CaO/Al_2O_3 ratio of ladle slag on formation behavior of inclusions in Mn and V alloyed steel, *ISIJ Int.*, 58(2018), No. 1, p. 88.
- [10] Y. Ren and L.F. Zhang, Thermodynamic model for prediction of slag–steel–inclusion reactions of 304 stainless steels, *ISIJ Int.*, 57(2017), No. 1, p. 68.
- [11] Y. Ren, L.F. Zhang, W. Fang, S.J. Shao, J. Yang, and W.D. Mao, Effect of slag composition on inclusions in Si-deoxidized 18Cr–8Ni stainless steels, *Metall. Mater. Trans. B*, 47(2016),

- No. 2, p. 1024.
- [12] A. Harada, G. Miyano, N. Maruoka, H. Shibata, and S.Y. Kitamura, Dissolution behavior of Mg from MgO into molten steel deoxidized by Al, *ISIJ Int.*, 54(2014), No. 10, p. 2230.
- [13] Y.S. Zou, A. Huang, L.P. Fu, and H.Z. Gu, Effect of lightweight refractories on the cleanness of bearing steels, *Ceram. Int.*, 44(2018), No. 11, p. 12965.
- [14] C.Y. Liu, F.X. Huang, J.L. Suo, and X.H. Wang, Effect of magnesia-carbon refractory on the kinetics of MgO-Al₂O₃ spinel inclusion generation in extra-low oxygen steels, *Metall. Mater. Trans. B*, 47(2016), No. 2, p. 989.
- [15] C.Y. Liu, F.X. Huang, and X.H. Wang, The effect of refining slag and refractory on inclusion transformation in extra low oxygen steels, *Metall. Mater. Trans. B*, 47(2016), No. 2, p. 999.
- [16] M.C. Mantovani, L.R. Moraes, R. Leandro da Silva, E.F. Cabral, E.A. Possente, C.A. Barbosa, and B.P. Ramos, Interaction between molten steel and different kinds of MgO based tundish linings, *Ironmaking Steelmaking*, 40(2013), No. 5, p. 319.
- [17] X.Y. Gao, L. Zhang, X.H. Qu, X.W. Chen, and Y.F. Luan, Effect of interaction of refractories with Ni-based superalloy on inclusions during vacuum induction melting, *Int. J. Miner. Metall. Mater.*, 27(2020), No. 11, p. 1551.
- [18] Y.S. Zou, A. Huang, L.P. Fu, P.F. Lian, Y.J. Wang, and H.Z. Gu, Chemical interactions between a calcium aluminate glaze and molten stainless steel containing alumina inclusions, *Ceram. Int.*, 44(2018), No. 1, p. 1099.
- [19] M. Song, M. Nzotta, and S.C. Du, Study of the formation of non-metallic inclusions by ladle glaze and the effect of slag on inclusion composition using tracer experiments, *Steel Res. Int.*, 80(2009), No. 10, p. 753.
- [20] Y.S. Lee, S.M. Jung, and D.J. Min, Interfacial reaction between Al₂O₃-SiO₂-C refractory and Al/Ti-killed steels, *ISIJ Int.*, 54(2014), No. 4, p. 827.
- [21] Y. Li, C.Y. Chen, G.Q. Qin, Z.H. Jiang, M. Sun, and K. Chen, Influence of crucible material on inclusions in 95Cr saw-wire steel deoxidized by Si-Mn, *Int. J. Miner. Metall. Mater.*, 27(2020), No. 8, p. 1083.
- [22] J.H. Shin, Y. Chung, and J.H. Park, Refractory-slag-metal-inclusion multiphase reactions modeling using computational thermodynamics: Kinetic model for prediction of inclusion evolution in molten steel, *Metall. Mater. Trans. B*, 48(2017), No. 1, p. 46.
- [23] W.L. Wang, L.W. Xue, T.S. Zhang, L.J. Zhou, H.P. Liu, H.G. Xiao, and Q.B. Sun, The influence of MgO/ZrO₂/Al₂O₃ refractories on the refining process of Ti-containing steel based on kinetic study, *Ceram. Int.*, 46(2020), No. 11, p. 17561.
- [24] Y. Zhang, Y. Ren, and L.F. Zhang, Modeling transient evolution of inclusion in Si-Mn-killed steels during the ladle mixing process, *Metall. Res. Technol.*, 114(2017), No. 3, art. No. 308.
- [25] Y. Zhang, Y. Ren, and L.F. Zhang, Kinetic study on compositional variations of inclusions, steel and slag during refining process, *Metall. Res. Technol.*, 115(2018), No. 4, art. No. 415.
- [26] L.G. Zhu, Y.N. Jia, Z.X. Liu, C.J. Zhang, X.J. Wang, and P.C. Xiao, Mass-transfer model for steel, slag, and inclusions during ladle-furnace refining, *High Temp. Mater. Processes*, 37(2018), No. 7, p. 665.
- [27] A. Harada, N. Maruoka, H. Shibata, and S.Y. Kitamura, A kinetic model to predict the compositions of metal, slag and inclusions during ladle refining: Part 1. basic concept and application, *ISIJ Int.*, 53(2013), No. 12, p. 2110.
- [28] S. Ohguchi, D.G.C. Robertson, B. Deo, P. Grieveson, and J.H.E. Jeffes, Simultaneous dephosphorization and desulphurization of molten pig iron, *Ironmaking Steelmaking*, 11(1984), No. 4, p. 202.
- [29] M. Hino and K. Ito, *Thermodynamic Data for Steelmaking*, Tohoku University Press, Tohoku, 2010, p. 259.
- [30] C. Wagner, *Thermodynamics of Alloys*, Addison-Wesley Pub. Co, Cambridge, 1962, p. 51.
- [31] C.H.P. Lupis and J.F. Elliott, Generalized interaction coefficients: Part I: Definitions, *Acta Metall.*, 14(1966), No. 4, p. 529.
- [32] G.K. Sigworth and J.F. Elliott, The thermodynamics of liquid dilute iron alloys, *Met. Sci.*, 8(1974), No. 1, p. 298.
- [33] H. Suito and R. Inoue, Thermodynamics on control of inclusions composition in ultraclean steels, *ISIJ Int.*, 36(1996), No. 5, p. 528.
- [34] J.J. Wang, L.F. Zhang, T.J. Wen, Y. Ren, and W. Yang, Kinetic prediction for the composition of inclusions in the molten steel during the electroslag remelting, *Metall. Mater. Trans. B*, 52(2021), No. 3, p. 1521.
- [35] J. Zhang, Calculating model of mass action concentrations for the slag system MnO-SiO₂, *J. Univ. Sci. Technol. Beijing*, 8(1986), No. 4, p. 1.
- [36] X.M. Yang, C.B. Shi, M. Zhang, G.M. Chai, and F. Wang, A thermodynamic model of sulfur distribution ratio between CaO-SiO₂-MgO-FeO-MnO-Al₂O₃ slags and molten steel during LF refining process based on the ion and molecule coexistence theory, *Metall. Mater. Trans. B*, 42(2011), No. 6, p. 1150.
- [37] S.C. Duan, C. Li, X.L. Guo, H.J. Guo, J. Guo, and W.S. Yang, A thermodynamic model for calculating manganese distribution ratio between CaO-SiO₂-MgO-FeO-MnO-Al₂O₃-TiO₂-CaF₂ ironmaking slags and carbon saturated hot metal based on the IMCT, *Ironmaking Steelmaking*, 45(2018), No. 7, p. 655.
- [38] A. Harada, N. Maruoka, H. Shibata, and S.Y. Kitamura, A kinetic model to predict the compositions of metal, slag and inclusions during ladle refining: Part2. condition to control inclusion composition, *ISIJ Int.*, 53(2013), No. 12, p. 2118.
- [39] L.P. Fu, H.Z. Gu, A. Huang, Y.S. Zou, and H.W. Ni, Enhanced corrosion resistance through the introduction of fine pores: Role of nano-sized intracrystalline pores, *Corros. Sci.*, 161(2019), art. No. 108182.
- [40] L. Fu, Y.S. Zou, A. Huang, H.Z. Gu, and H.W. Ni, Corrosion mechanism of lightweight microporous alumina-based refractory by molten steel, *J. Am. Ceram. Soc.*, 102(2019), No. 6, p. 3705.
- [41] P.V. Danckwerts, Kinetics of the absorption of carbon dioxide in water, [in] *Insights into Chemical Engineering*, Elsevier, Amsterdam, 1981, p. 5.
- [42] J.H. Wei and A. Mitchell, Changes in composition during A. C.ESR—I. Theoretical development, *Acta Metall. Sin.*, 20(1984), No. 5, p. 387.
- [43] D. Hou, Z.H. Jiang, Y.W. Dong, W. Gong, Y.L. Cao, and H.B. Cao, Effect of slag composition on the oxidation kinetics of alloying elements during electroslag remelting of stainless steel: Part-1 mass-transfer model, *ISIJ Int.*, 57(2017), No. 8, p. 1400.
- [44] D. Hou, Z.H. Jiang, Y.W. Dong, Y. Li, W. Gong, and F.B. Liu, Mass transfer model of desulfurization in the electroslag remelting process, *Metall. Mater. Trans. B*, 48(2017), No. 3, p. 1885.
- [45] W.T. Lou and M.Y. Zhu, Numerical simulation of desulfurization behavior in gas-stirred systems based on computation fluid dynamics-simultaneous reaction model (CFD-SRM) coupled model, *Metall. Mater. Trans. B*, 45(2014), No. 5, p. 1706.
- [46] J.C. Lamont and D.S. Scott, An eddy cell model of mass transfer into the surface of a turbulent liquid, *AIChE J.*, 16(1970), No. 4, p. 513.